Co-Continuous Composite Materials for Stiffness, Strength, and Energy Dissipation

*Lifeng Wang, Jacky Lau, Edwin L. Thomas, and Mary C. Boyce**

Two-component ordered structures in which both phases are solid and continuous (co-continuous solid structures) are unusual in nature and in commercial applications. Natural and synthetic co-continuous structures, comprised of hard and soft materials can provide outstanding combinations of properties including stiffness, strength, impact resistance, toughness, and energy dissipation.[1,2] The geometric and topological arrangement of the constituents provides avenues to engineer the macroscale properties. Various chemical processing routes and technologies now enable the precise production of ordered co-continuous microstructured materials over a wide range of length scales. For example, block copolymer chemistry can be tailored to provide periodic bi-continuous structures with feature size of sub-micrometer[3] while immiscible polymer blends can yield random bi-continuous structures.[4] Solid co-continuous microstructures in other material systems have also been of recent interest, including metal-ceramic composites[5] and metallic glass matrix composites.[6] In this paper, we demonstrate the potential to design and fabricate co-continuous glassy polymer/rubbery polymer materials with enhancements in stiffness, strength and energy dissipation using a 3D printer with sub-millimeter feature size.

The model systems of co-continuous polymer composites we study here are based on microstructures which possess interfaces close to those of triply periodic minimal surfaces. These structures have been of great interest to mathematicians, physical scientists, material scientists, and biologists. Close physical approximations to triply periodic minimal surfaces arise in a few material systems, such as block copolymers,[3,7] micellar materials,[8] nanocomposites,[9] and biological exoskeletons.[10,11] Recent theoretical studies have shown that bicontinuous two-phase composites with minimal interface structures exhibit optimal simultaneous thermal and electrical conductivity[12] as well as optimal multi-functional properties such as a combination of a high bulk modulus together with a high electrical (or thermal) conductivity.[13] Recent investigations of periodic porous cellular microframes have demonstrated that level set equations are useful analytical approximations to minimal surfaces and can be parameterized to systematically explore families of surfaces with fixed symmetries but variable volume fractions and surface curvature. Level set structures can provide better elastic properties compared to their corresponding rod-connected counterparts due to the effect of curvature in the ligaments.[14] Furthermore, these structures can be scaled down (or up) and fabricated; for example using photolithography for sub-micrometer length scale structures that enable the coupling of mechanical deformation with photonic or phononic properties,[11,14,15] i.e. the creation of mechanically tunable photonic or phononic band gap materials.[16,17] Therefore, the relationship between macroscopic mechanical response and constituent material properties and geometric arrangement holds great promise in the multifunctional design of engineering structures and materials and even metamaterials.[18]

In this paper, we consider three types of co-continuous structures with simple cubic (SC), body-centered-cubic (BCC), and face-centered cubic (FCC) Bravais lattices (see **Figure 1**) described by Equations 1–3 from Reference 14, which correspond to the level set structures associated with triply periodic minimal surfaces known as P, I-WP, and F-RD,[19,20] respectively. We compute the linear and nonlinear mechanical behavior of the level set structures including their elastic stiffness, yield, post-yield, and dissipative behaviors. We also fabricate certain level set structures using a 3D printing process and experimentally measure their mechanical behavior. The properties obtained for these co-continuous structures are compared with conventional particle-reinforced composites (PC), fiber-reinforced composites (FC), and lamellar composites (LC).

Figure 1 displays the 3D periodic SC, BCC, and FCC co-continuous structures under consideration where the volume fraction of each phase is set to 50%. We investigate the elastic-plastic mechanical response of these composites using finite element analysis (FEA) of micromechanical models of representative volume elements (RVEs) for each microstructure, varying the relative volume fractions of each phase.[21,22] The constituent phases A and B are taken to be either a representative glassy polymer or a representative elastomer material. The stress-strain behavior of the glassy polymer is captured using an elastic-viscoplastic model[23–25] which includes the classic features of initial linear elasticity, yielding, post-yield strain softening, and subsequent strain hardening at larger strains (see Supporting Information). The set of material constants is taken from a glassy, crosslinked epoxy material, SU-8[26] with a Young's modulus of 3.30 GPa, Poisson's ratio of 0.33, and a yield stress of 105 MPa. The elastomeric stress-strain behavior is modeled as a nearly incompressible neo-Hookean material with shear modulus of 3.3 MPa and bulk modulus of 1.0 GPa.

Dr. L. F. Wang, J. Lau, Prof. M. C. Boyce
Department of Mechanical Engineering
Massachusetts Institute of Technology
Cambridge, MA 02139, USA
E-mail: mcboyce@mit.edu
Prof. E. L. Thomas
Institute for Soldier Nanotechnologies
Department of Materials Science and Engineering
Massachusetts Institute of Technology
Cambridge, MA 02139, USA

DOI: 10.1002/adma.201003956

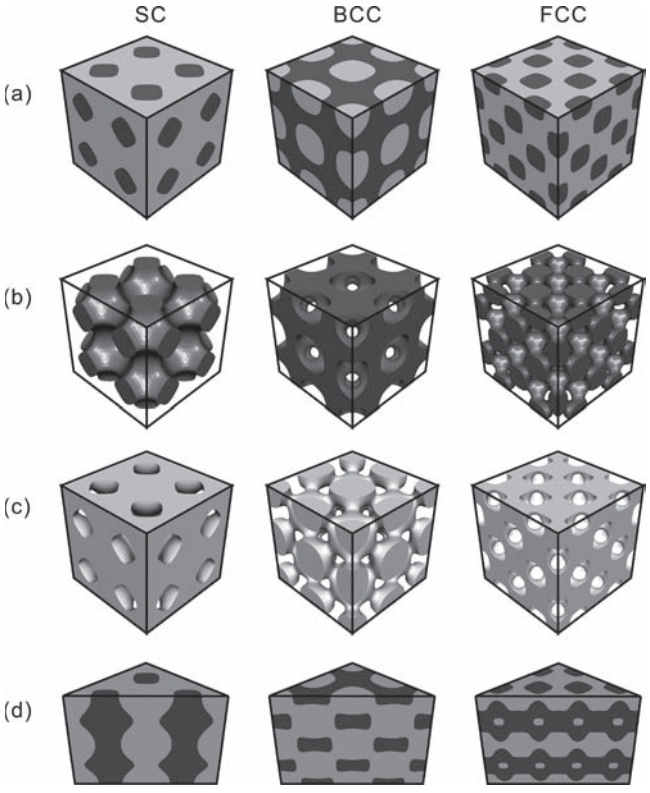

Figure 1. (a) 3D periodic co-continuous composites consisting of 2 × 2 × 2 unit cells with simple cubic lattice, body-centered-cubic lattice, and face-centered-cubic lattice. (b) The corresponding phase A in these composites. (c) The corresponding phase B in these composites. Phase A and B are separated by intermaterial dividing surfaces of level set structures.[14] (d) The corresponding cross-section in diagonal view.

Mechanical properties were experimentally measured for the BCC structures with 50%/50%, 35%/65%, and 65%/35% glassy A/rubbery B phase content using glassy/rubbery 3D printable materials.

Figure 2 depicts the simulated mechanical response of the glassy polymer/elastomer co-continuous composites of Figure 1 during uniaxial compression. The true stress-true strain curves of these composites exhibit initial linear elasticity, followed by yield and post-yield strain hardening (Figure S3). Figures 2a, 2c, and 2d show the effects of volume fraction on the composite Young's modulus, yield stress, and energy absorption (which we compute as the work after 25% axial strain) for the case of <100> uniaxial compression on each of the structures. At any given volume fraction, the SC composites provide a higher <100> Young's modulus, yield stress and energy absorption ability than either tahe BCC or FCC structures. The SC structure possesses an axially oriented columnar glassy region – which supports load in direct compression deformation giving the stiffer, stronger behavior as compared to the FCC structure which carries the <100> loading primarily through bending/shear deformation of the constituents. Furthermore, for each structure, the elastomer enhances the mechanical response due to its support and constraint on the glassy polymer phase which increases and further distributes the stress level in the glassy regions. Figure 2e shows the comparison of the von Mises stress, axial stress and axial strain contours of the co-continuous composites and the corresponding glassy polymer/air porous structures, showing that glassy polymers contribute more significantly to the stress response (and hence enhance the stiffness) in co-continuous solid/solid composites.

For the cubic structures there are three independent elastic constants. The Zener anisotropy ratio $A = 2C_{44}/(C_{11} - C_{12})$ is used to characterize the elastic anisotropy of these structures, where the three C_{ij} denote the three independent Voigt elastic stiffness coefficients.[27] The Zener ratio reflects the ratio of the shear modulus (in the cubic axis system) of the anisotropic cubic structure, $2C_{44}$, to that of an isotropic material possessing the same extension/contraction behavior (C_{11}, C_{12}) of the cubic material. For isotropic materials, $A = 1$. Figure 2b depicts the anisotropy ratio as a function of the volume fraction for SC, BCC, and FCC composites, indicating strong dependence on the volume fraction as expected. It is found the anisotropy ratio A is close to 1 for the composites with 50%/50% volume contents. Additional effects of anisotropy on modulus as well as on yield stress and energy absorption are discussed later.

The composite elastic modulus and yield stress are dominated by the glassy polymer phase in the composites and the scaling laws generally used for cellular structures[1] may be used to assess the response of these co-continuous composites. For example, the Young's modulus, E^*, of the composite can be described as a function of solid polymer modulus, E_s, and the relative volume of the glassy polymer, $\upsilon_f = V^*/V$, via $E^* = CE_s(\upsilon_f)^n$ where C and n can be obtained by fits to experimental data. The scaling exponent n close to 1 indicates stretch-dominated deformation behavior of the ligaments whereas an exponent of 2 typically indicates bending-dominated deformation.[28] Various cellular materials have been found to exhibit different scaling exponents such as metal foams (n ~ 1–3),[29] ordered nanoporous silica (n ~ 0.6–1),[30] and periodic epoxy nanoframes (n ~ 1.26).[31] Considering the case where phase A is the glassy polymer (phase B is the elastomer) and axial loading along the <100> direction, it is found that n = 1.2 for SC composites, n = 1.03 for BCC composites, and n = 2.3 for FCC composites (for volume fractions of the glassy polymer ranging from 20% to 70%). This implies SC and BCC composites are close to "stretch-dominated" while FCC composites are more "bending-dominated" when axially loaded in the <100> direction. As discussed earlier, the stretch-dominated aspect of SC and BCC composites are due to the "columnar" regions along <100> which are not present in the FCC as was evident in σ_{22} contours in Figure 2e. When the composites are axially loaded in the <111> direction, it is found that n = 1.84 for SC composites, n = 2.31 for BCC composites, and n = 1.79 for FCC composites, indicating more bending-dominated deformation occurs in SC and BCC composites when loaded in the <111> direction. Interestingly, the scaling exponent n is smaller in the two-material co-continuous composites compared to the porous counterparts, indicating less loss in elastic stiffness when decreasing the volume fraction of the glassy phase (Table S2). Similar trends hold for the yield stress. Moreover, the energy dissipation values for compression to 25% strain vary from 7–12 MJ/m^3 for co-continuous composites with 50%/50% volume distribution, depending on the microstructure. Note that

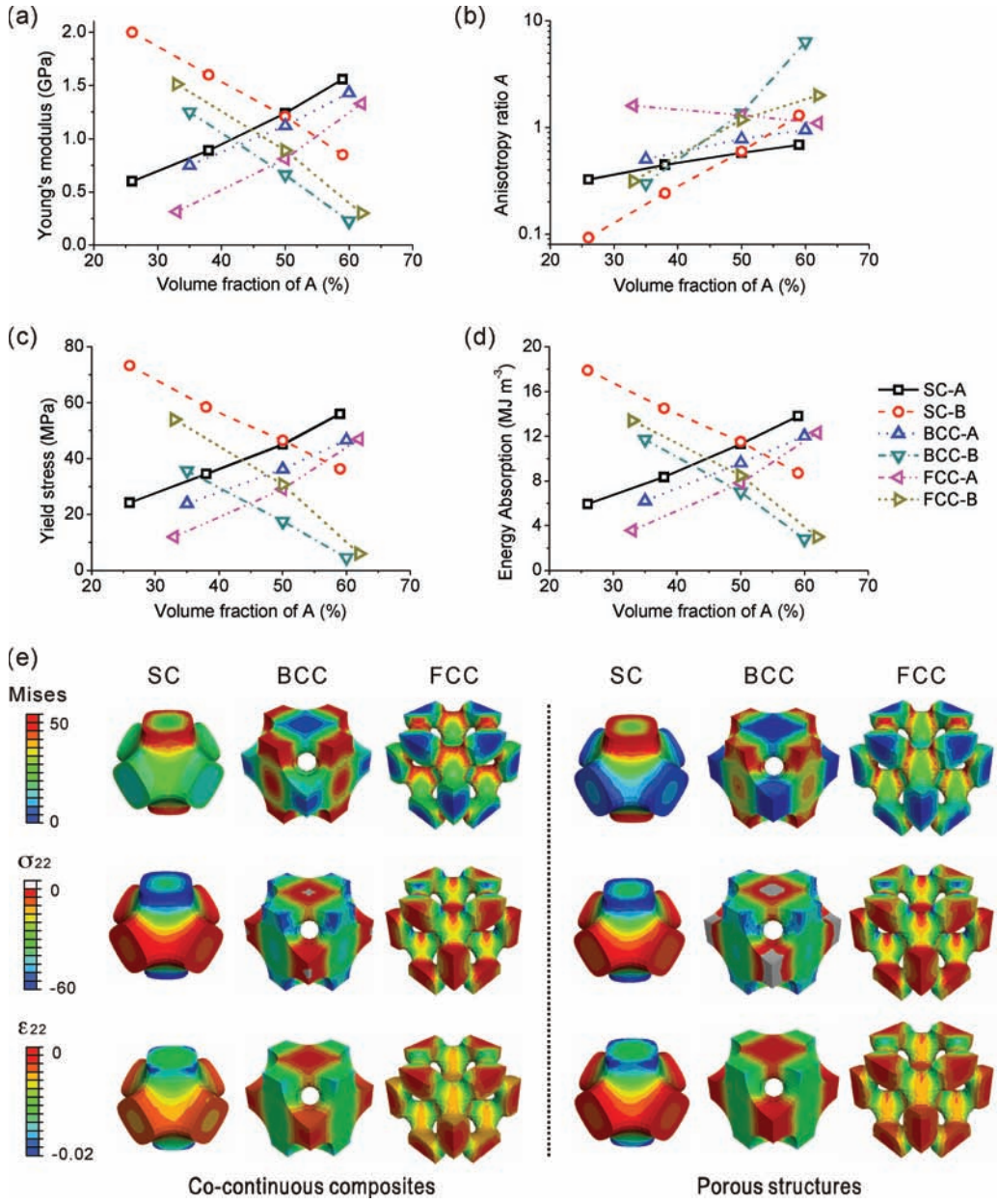

Figure 2. Mechanical response of the glassy polymer/elastomer co-continuous composites. (a–d) Young's modulus, anisotropy ratio, yield stress and energy absorption dissipation at 25% strain of co-continuous composites with varying volume fraction of phase A. (e) von Mises stress (MPa), axial stress (MPa), and axial strain contours of three co-continuous composites (left) (50% volume fraction, only glassy polymer phase is shown) and the corresponding porous structures (right) at a macroscopic compression strain of 1%.

the average density of the co-continuous composites is ~1050–1200 kg/m^3, depending on the volume fraction of each phase; the specific energy absorption could be as high as 6–11 MJ/Mg. This value rates among the highest values reported for commercially available polymer foams.[1] The stress contours in the post-yield region (see Figure S3c) reveal that a greater volume of material yields in the co-continuous composites as compared to the corresponding glassy/air structures. This energy dissipation capability implies that the co-continuous composites can be tailored to provide enhanced dissipation mechanisms that engage more of the material in plastic deformation.

In order to study the co-continuous polymer composites experimentally, representative BCC structures are fabricated and tested at the sub-millimeter scale. The polymer/elastomer co-continuous composites were fabricated using the Connex500 3D printer (Objet Geometries, USA) which allows the simultaneous printing of two different materials. TangoPlus (a rubber-like flexible material) and VeroWhite (an acrylic-based photopolymer) were used in the composites.[32] **Figures 3**a and 3b show the representative 50%/50% BCC composites consisting of 4 × 4 × 4 unit cells fabricated via 3D printing. Three samples for each volume fraction of BCC composite were tested using a

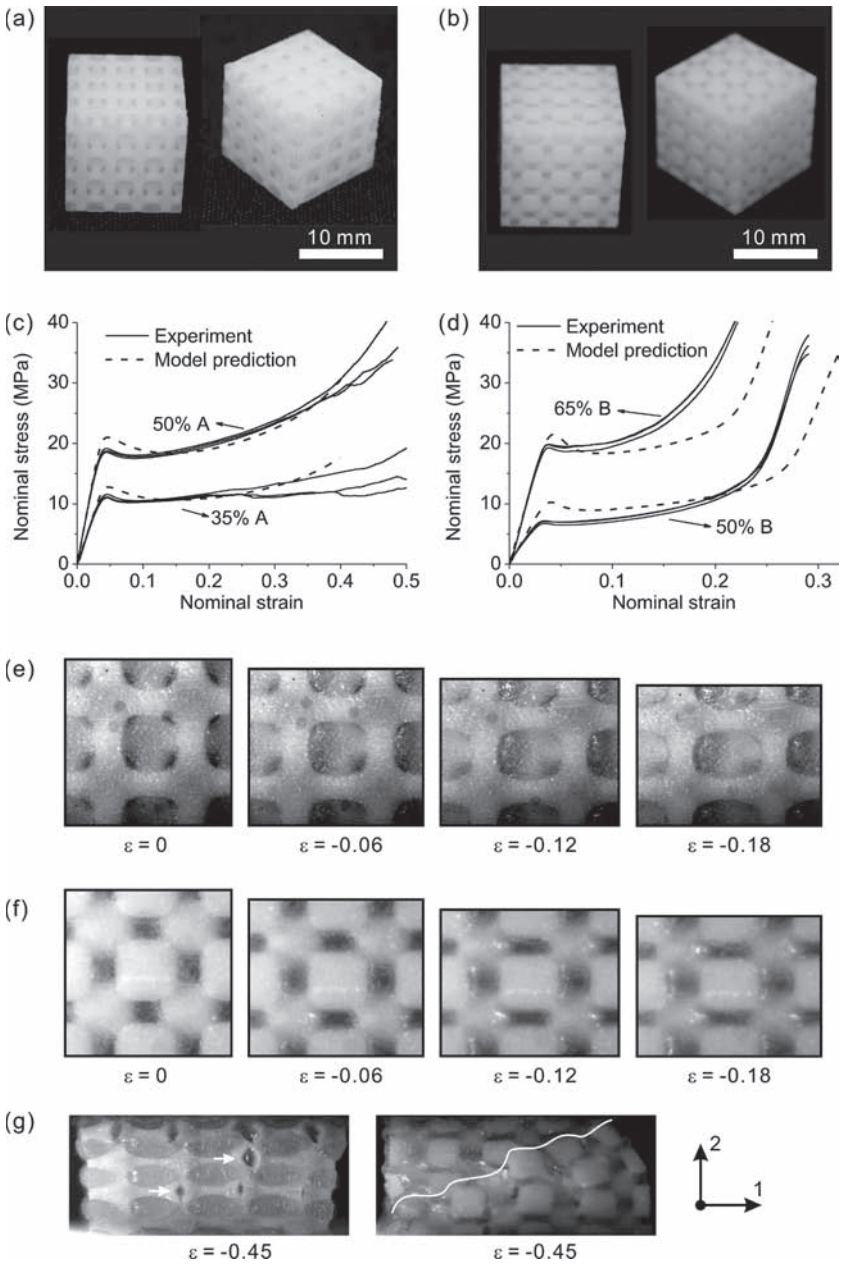

Figure 3. Experimental study of BCC co-continuous composites. (a,b) BCC co-continuous composites with 50% volume fraction of each phase fabricated through 3D printing where glassy polymer is white and elastomer is transparent: (a) phase A is glassy polymer; (b) phase B is glassy polymer. (c,d) Nominal stress–strain curves showing comparison of simulation result and 3 experimental tests at two volume fractions: (c) 35% and 50% of glassy polymer phase A; (d) 50% and 65% of glassy polymer phase B. (e,f) Experimental images of BCC composites at different levels of macroscopic strain: 0, –0.06, –0.12, and –0.18. (g) Deformed configuration under a compression strain of 0.45 showing cracking contained in the glassy polymer (arrows in left figure) for the case phase A is the glassy polymer and global shear failure (right) for the case phase B is the glassy polymer. The line indicates location of shear band.

Zwick Mechanical Tester (Zwick Z010, Zwick Roell, Germany). The nominal stress- nominal strain curves show the repeatability up to 40% compression strain as shown in Figure 3c and 3d at a strain rate of 0.01 s^{-1}. The simulation results consider the stress-strain behaviors of the 3D printed constituent materials (see Supporting Information) together with the microstructure geometries and are found to be highly predictive of the behavior of the co-continuous composites (see Table S3 for the comparison between simulated and experimental results). The simulated yield stresses are slightly higher than the corresponding experimental values most likely due to the fidelity of the 3D print process. Although Connex500 has a stated resolution of ~30 μm, the accuracy can still affect the volume fraction and distribution of each phase. As expected, the composites with greater content of glassy polymer provide higher Young's modulus and yield stress. For the composites where phase B is the glassy polymer, the yield stress is increased by a factor of 2.7 (for experiments and 2.1 for simulations) when the glassy polymer content changes from 50% to 65%. At larger strains (>25%), cracking is observed to occur in the interior of a glassy polymer region rather than at an interface between phases (see Figure 3g left). However, these cracks do not reduce the stress level significantly, but are evident by the drops in the experimental stress-strain curves in Figure 3c. The co-continuity of the structure constrains the cracking and enables these composites to provide energy absorption to larger strains before catastrophic failure. For the BCC composite where phase B is the glassy polymer, cracking is not observed, instead a global shear failure occurs (see Figure 3g right). Thus, for this composite, strain hardening curves are smooth in all experimental tests (Figure 3d) while the failure strain is smaller as compared to the case in Figure 3c. Moreover, experimental curves harden at lower strain than the model prediction because localized shear deformation occurs in the finite sized samples in the experiment and this is suppressed in the simulations due to the periodic nature of the RVE. These results suggest good ability to tailor the microstructure to achieve different failure mechanisms to enhance energy dissipation under large deformation.

The stress transfer and strain sharing mechanisms are particularly important for the co-continuous composites with a brittle component since the continuous elastomer phase constrains the brittle phase which increases the macroscopic failure strain by both limiting crack propagation and enabling a multitude of cracking events. The ε_{11} strain contour in Figure S4 shows a positive value in the center of the glassy polymer at large strain which explains the observation of multiple cracking in these regions at large compressive strain (Figure 3g left) with the cracks oriented parallel to the axis of applied compression. None of these cracks catastrophically propagated, but

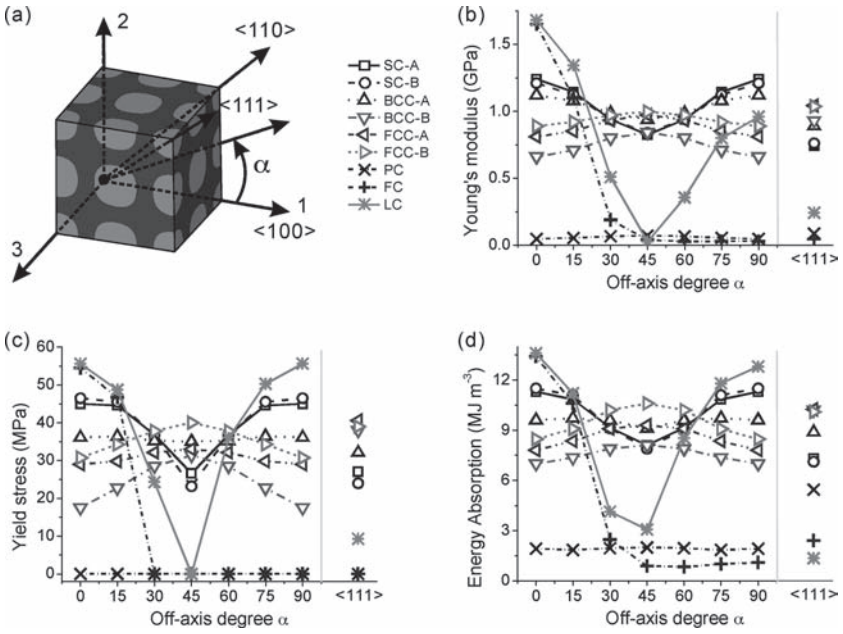

Figure 4. Mechanical response of the particle-reinforced composites (PC), fiber-reinforced composites (FC), lamellar composites (LC), SC, BCC, and FCC co-continuous composites under uniaxial compression as a function of off-axis loading angle in the 12 plane and in the <111> direction (right column): (a) schematic of the loading direction (b) Young's modulus; (c) yield stress (0 presents the case without apparent yielding); (d) energy absorption dissipation at 25% strain. Here the volume fraction of each phase is fixed to be 50% for all composites.

instead cracks were found to initiate at all of the equivalent locations within the microstructure. The cracking mechanism provides additional energy dissipation. The mutual support of the two co-continuous phases provides load transfer even in the face of cracking and imparts damage tolerance.

Anisotropy is another interesting property for structural materials and composites. Anisotropy can be used to advantage, however it can also cause unexpected failure if the structure or material has a very compliant and weak loading resistance in any direction. To investigate the anisotropy of the set of co-continuous composites, FEA simulations are conducted on RVEs subjected to systematic off- <100> axis loadings (see **Figure 4** schematic). Young's modulus, axial yield stress, and energy absorption at 25% compression strain are computed from the uniaxial compression simulations in different orientations and are shown in Figure 4b–d, respectively. To evaluate the results for SC, BCC, and FCC composites, the anisotropy degree is defined as the ratio of the minimum value/maximum value for each of the Young's modulus, yield stress, or energy absorption. The calculated anisotropy degree varies from 0.66–0.9(Young's modulus), 0.5–0.97(yield stress), 0.69–0.95(energy absorption), depending on the co-continuous microstructure. For instance, the BCC composites where phase A is the glassy polymer have an anisotropy degree of 0.80, 0.88, and 0.92 for Young's modulus, yield stress, and energy absorption, respectively, which can be considered a quasi-isotropic material. This is consistent with the Zener anisotropy ratio shown in Figure 2b, where the BCC and FCC composites with 50%/50% volume content are close to isotropic materials ($A = 1$). From similar simulations conducted on the conventional PC, FC, and LC composites with the same constituent material properties and volume fraction, the lowest modulus anisotropy degree is 0.65, 0.016, and 0.016, respectively. Although FC and LC composites have a higher modulus and yield stress in the direction parallel to the fiber axis or lamellar plane, the off-axis loading simulations show relatively poor mechanical behavior. As is well known, this is a limitation in use of conventional composites in applications that have off-axis loading conditions that typically forces the construction of cross-ply laminates with lamellae of different orientations. Compared to the conventional composites, the co-continuous composites are 3D multi-directionally reinforced, are less dependent on material distribution, and simultaneously provide relatively high stiffness, strength and energy absorption in all directions. These properties suggest co-continuous composites as excellent energy dissipative elements in advanced structures or armor by controlling volume fraction and tailoring geometric arrangements to meet different requirements.[33–35]

In summary, we have investigated the macroscopic mechanical response of 3D periodic glassy polymer/elastomer co-continuous composites with different geometric arrangements of the constituents through simulations and experiments. We have shown that 3D periodic co-continuous composites can have enhanced mechanical performance achieving a unique combination of stiffness, strength and energy absorption as compared to the conventional particle-reinforced composites, fiber-reinforced composites, and lamellar composites. Of particular note, the mutual constraints between two phases of the co-continuous structure enable enhanced dissipation by spreading of the plastic deformation and by containing cracking leading to a multitude of non-catastrophic dissipative events, which also provides damage tolerance of the co-continuous composites. These results provide guidelines for engineering and tailoring the nonlinear mechanical behavior and energy absorption of co-continuous composites for a wide range of applications and further creating multifunctional materials. For example, polymeric materials which can change shape and material properties in response to external stimuli, such as a temperature or electric field, can provide additional functionality when used as one of the phases. Polymer co-continuous composites also provide the potential of 3D shape memory or tailored viscoelastic behavior where the two phases can be chosen to tune the shape memory or the viscoelastic behaviors to be activated at multiple temperatures and/or multiple time scales. The periodic and multiphase nature of the structures also enable mechanically tunable band gap (phononic or photonic) materials, and tunable sensors in tissue engineering. While the feature lengthscale of the current study is at the millimeter scale, these results extend down to micron or sub-micron lengthscales where fabrication challenges can be met with innovative lithography[15] and other processing

techniques such as block copolymer for periodic structures.[3,36] At these smaller scales, further property enhancement may result due to lengthscale effect on, for example strength and ductility.[16,26] Ongoing and future research addresses the study of the shape memory effect, thermal and electrical conductivity, and opportunities at different lengthscales.

Experimental Section

The polymer/elastomer co-continuous composites were fabricated using the Connex500 3D printer (Objet Geometries, MA, USA) that allows the simultaneous printing of two different materials. TangoPlus (a rubber-like flexible material) and VeroWhite (an acrylic-based photopolymer) were used in the composites; the chemistry of these materials is proprietary to Objet Geometries. The elastomer (TangoPlus) has shear modulus 0.213 MPa and density of 1141 kg/m^3; the glassy polymer (VeroWhite) has Young's modulus 1.8 GPa, yield stress 75 MPa and density of 1174 kg/m^3. The stress–strain behavior of these constituent materials is provided in the Supporting Information. Input level set based structural geometries were prepared in a CAD software (SolidWorks 2009, Dassault Systèmes SolidWorks Corp., Massachusetts, USA) and then exported as Stereolithography files (in STL format) for direct printing in the Connex500. Preset composites of model materials were jetted from designated nozzles in ultra-thin layers onto a build tray. Each photopolymer layer was cured by UV light immediately after it was jetted, producing fully cured models. Each composite sample consists of $4 \times 4 \times 4$ unit cells with a periodicity of ~3.5 mm. The sample height is 14 mm and the feature size is ~500 μm. The stated resolution of the Connex500 is ~30 μm. The as-fabricated composites were then kept at room condition for 7 days to allow for saturation of curing.

Tensile tests were conducted using a Zwick Mechanical Tester (Zwick Z010, Zwick Roell, Germany). The compression tests were conducted at a strain rate of 0.01 s^{-1}. The load was measured with a 10kN load cell.

Supporting Information

Supporting Information is available from the Wiley Online Library or from the author.

Acknowledgements

This research was supported by the U.S. Army through the Institute for Soldier Nanotechnologies (ISN), under contract W911NF-07-D-0004.

Received: October 26, 2010
Revised: December 20, 2010
Published online: February 25, 2011

[1] L. J. Gibson, M. F. Ashby, *Cellular Solids: Structure and Properties*, 2nd ed., Cambridge University Press, Cambridge **1999**.
[2] M. F. Ashby, *Materials Selection in Mechanical Design*, 3rd ed., Butterworth-Heinemann, Oxford **2005**.
[3] E. L. Thomas, D. M. Anderson, C. S. Henkee, D. Hoffman, *Nature* **1988**, *334*, 598.
[4] a) L. A. Utracki. *Polymer alloys and blends*, Hanser Gardner Publications, Munich **1989**; b) R. Lehman, J. Idol, T. Nosker, R. Renfree, J. Lynch, K. Van Ness, US Patent Application 20060134157, **2006**.
[5] a) X. F. Zhang, G. Harley, L. C. De Jonghe, *Nano Lett.* **2005**, *5*, 1035; b) R. Dzugan, B. P. Bardes, US Patent Application 20070009754, **2007**.
[6] D. C. Hofmann, J. Y. Suh, A. Wiest, G. Duan, M. L. Lind, M. D. Demetriou, W. L. Johnson, *Nature* **2008**, *451*, 1085.
[7] P. D. Olmstead, S. T. Milner, *Macromolecules* **1998**, *31*, 4011.
[8] P. Ziherl, R. D. Kamien, *Phys. Rev. Lett.* **2000**, *85*, 3528.
[9] Y. Lu, Y. Yang, A. Sellinger, M. Lu, J. Huang, H. Fan, R. Haddad, G. Lopez, A. R. Burns, D. Y. Sasaki, J. Shelnutt, C. J. Brinker, *Nature* **2001**, *410*, 913.
[10] S. T. Hyde, S. Andersson, K. Larsson, Z. Blum, T. Landh, S. Lidin, B. W. Ninham, *The Language of Shape*, Elsevier Science B.V., Amsterdam **1997**.
[11] Y.-H. Ha, R. A. Vaia, W. F. Lynn, J. P. Costantino, J. Shin, A. B. Smith, P. T. Matsudaira, E. L. Thomas, *Adv. Mater.* **2004**, *16*, 1091.
[12] S. Torquato, S. Hyun, A. Donev, *Phys. Rev. Lett.* **2002**, *89*, 266601.
[13] S. Torquato, A. Donev, *Proc. R. Soc. London, Ser. A*, **2004**, *460*, 1849.
[14] M. Maldovan, C. K. Ullal, J.-H. Jang, E. L. Thomas, *Adv. Mater.* **2007**, *19*, 3809.
[15] M. Maldovan, E. L. Thomas, *Periodic Materials and Interference Lithography: for Photonics, Phononics and Mechanics*, Wiley-VCH Verlag GmbH & Co. KGaA, Weinheim **2009**.
[16] J.-H. Jang, C. K. Ullal, T. Gorishnyy, V. V. Tsukruk, E. L. Thomas, *Nano Lett.* **2006**, *6*, 740.
[17] K. Bertoldi, M. C. Boyce, *Phys. Rev. B* **2008**, *77*, 052105.
[18] N. Fang, D. Xi, J. Xu, M. Ambati, C. Sun, X. Zhang, *Nat. Mater.* **2006**, *5*, 452.
[19] M. Wohlgemuth, N. Yufa, J. Hoffman, E. L. Thomas, *Macromolecules* **2001**, *34*, 6083.
[20] A. H. Schoen, *NASA Technical Report*, TN D-5541, Washington, DC **1970**.
[21] M. Danielsson, D. M. Parks, M. C. Boyce, *J. Mech. Phys. Solids* **2002**, *50*, 351.
[22] M. Danielsson, D. M. Parks, M. C. Boyce, *J. Mech. Phys. Solids* **2007**, *55*, 533.
[23] M. C. Boyce, D. M. Parks, A. S. Argon, *Mech. Mater.* **1988**, *7*, 15.
[24] E. M. Arruda, M. C. Boyce, *Int. J. Plasticity* **1993**, *9*, 697.
[25] J. S. Bergstrom, M. C. Boyce, *J. Mech. Phys. Solids* **1998**, *46*, 931.
[26] L. F. Wang, M. C. Boyce, C.-Y. Wen, E. L. Thomas, *Adv. Funct. Mater.* **2009**, *19*, 1343.
[27] H. Ledbetter, A. Miglioria, *J. Appl. Phys.* **2006**, *100*, 063516.
[28] M. F. Ashby, *Philos. Trans. R. Soc. London, Ser. A* **2006**, *364*, 15.
[29] M. F. Ashby, A. G. Evans, N. A. Fleck, L. J. Gibson, J. W. Hutchinson, H. N. G. Wadley, in *Metal Foams: A Design Guide*, Butterworth-Heinemann, Boston **2000**.
[30] H. Fan, C. Hartshorn, T. Buchheit, D. Tallant, R. Assink, R. Simpson, D. J. Kissel, D. J. Lacks, S. Torquato, C. J. Brinker, *Nat. Mater.* **2007**, *6*, 418.
[31] J. H. Lee, L. F. Wang, S. Kooi, M. C. Boyce, E. L. Thomas, *Nano Lett.* **2010**, *10*, 2592.
[32] Objet Geometries, Inc. homepage, http://www.objet.com, Billerica, MA **2010**.
[33] P. J. Hogg, *Science* **2006**, *314*, 1100.
[34] L. F. Wang, M. C. Boyce, *Adv. Funct. Mater.* **2010**, *20*, 3025.
[35] N. V. David, X. -L. Gao, and J. Q. Zheng, *Appl. Mech. Rev.* **2009**, *62*, 050802.
[36] B. J. Dair, C. C. Honeker, D. B. Alward, A. Avgeropoulos, N. Hadjichristidis, L. J. Fetters, M. Capel, E. L. Thomas, *Macromolecules* **1999**, *32*, 8145.